Functional adaptation of the switch-2 nucleotide sensor enables rapid processive translocation by myosin-5

Nikolett T. Nagy,* Takeshi Sakamoto,[†,1] Balázs Takács,* Máté Gyimesi,* Eszter Hazai,[‡] Zsolt Bikádi,[‡] James R. Sellers,[†] and Mihály Kovács*,[2]

*Department of Biochemistry, Eötvös University, Budapest, Hungary; [†]Laboratory of Molecular Physiology, National Heart, Lung, and Blood Institute, Bethesda, Maryland, USA; and [‡]VirtuaDrug Ltd., Budapest, Hungary

ABSTRACT **Active site loops that are conserved across superfamilies of myosins, kinesins, and G proteins play key roles in allosteric coupling of NTP hydrolysis to interaction with track filaments or effector proteins. In this study, we investigated how the class-specific natural variation in the switch-2 active site loop contributes to the motor function of the intracellular transporter myosin-5. We used single-molecule, rapid kinetic and spectroscopic experiments and semiempirical quantum chemical simulations to show that the class-specific switch-2 structure including a tyrosine (Y439) in myosin-5 enables rapid processive translocation along actin filaments by facilitating Mg^{2+}-dependent ADP release. Using wild-type control and Y439 point mutant myosin-5 proteins, we demonstrate that the translocation speed precisely correlates with the kinetics of nucleotide exchange. Switch-2 variants can thus be used to fine-tune translocation speed while maintaining high processivity. The class-specific variation of switch-2 in various NTPase superfamilies indicates its general role in the kinetic tuning of Mg^{2+}-dependent nucleotide exchange.—Nagy, N.T., Sakamoto, T., Takács, B., Gyimesi, M., Hazai, E., Bikádi, Z., Sellers, J.R., Kovács, M. Functional adaptation of the switch-2 nucleotide sensor enables rapid processive translocation by myosin-5. *FASEB J.* 24, 4480–4490 (2010). www.fasebj.org**

Key Words: actomyosin · kinetics · nucleotide exchange · single molecule · sliding speed

IT IS NOW A WELL-ESTABLISHED concept that myosins, kinesins, G proteins, and several other superfamilies of NTPases use similar enzymatic mechanisms and homologous structural elements to harness the energy liberated during NTP hydrolysis for signal propagation, timing, or proofreading of biochemical processes or, in the case of molecular motors, producing mechanical work. A central aspect of these activities is the allosteric interplay between the NTPase active site and the binding site of a protein effector or track: this communication enables both the sensing of the nucleotide state and the enzymatic activation of the NTPase by the partner protein. In the case of linear motors such as myosin and kinesin, a cyclical change in track affinity during the NTPase cycle coupled to key conformational changes leads to unidirectional translocation along the track.

The most important conserved structural elements that enable allosteric coupling between the NTP and track or effector binding sites of the above NTPases include the P loop (also called N-1 or G-1), switch-1 (N-2 or G-2), and switch-2 (N-3 or G-3) (1, 2). In myosins, kinesins, and G proteins, the roles of the two broadly conserved residues in the switch-2 consensus sequence DXXG have been characterized in detail: the aspartate coordinates the Mg^{2+} ion of the MgNTP ligand through a water molecule, whereas the main chain of the glycine forms an interaction with the γ-phosphate of NTP that is essential for catalysis (**Fig. 1*A***) (3, 4). However, other positions in switch-2 that show intriguing class-specific variation patterns have received much less attention. The most striking example is the residue preceding the catalytic glycine, which may be important in positioning switch-2 and thus may influence nucleotide hydrolysis and exchange and, in turn, allosteric communication with binding partners (Fig. 1*A*). This hypothesis is even more tempting in light of the fact that the myosin-specific extended switch-2 consensus sequence LDIXGFE also displays class-specific variation in this position (Fig. 1*A*; see also below).

Members of the myosin superfamily of motors play essential roles in various cellular functions including muscle contraction, intracellular transport, cytokinesis, cell migration, differentiation, endo- and exocytosis, and formation of cell protrusions (5, 6). Myosins move along actin filaments using the energy of ATP hydrolysis catalyzed by their motor domain that contains the ATP- and actin-binding sites as well as the base of the lever arm (Fig. 1*B–D*). Besides members of the myosin-2 class including muscle myosins, the intracellular transporter myosin-5a has been investigated in great detail (7–9). In striking contrast to muscle myosin-2 that works in the large ensemble of the thick filament, myosin-5a performs pro-

[1] Current address: Department of Physics and Astronomy, Wayne State University, Detroit, MI 48201, USA.

[2] Correspondence: Department of Biochemistry, Eötvös University, H-1117 Budapest, Pázmány P. stny. 1/C, Hungary. E-mail: kovacsm@elte.hu

doi: 10.1096/fj.10-163998

0892-6638/10/0024-4480 © FASEB

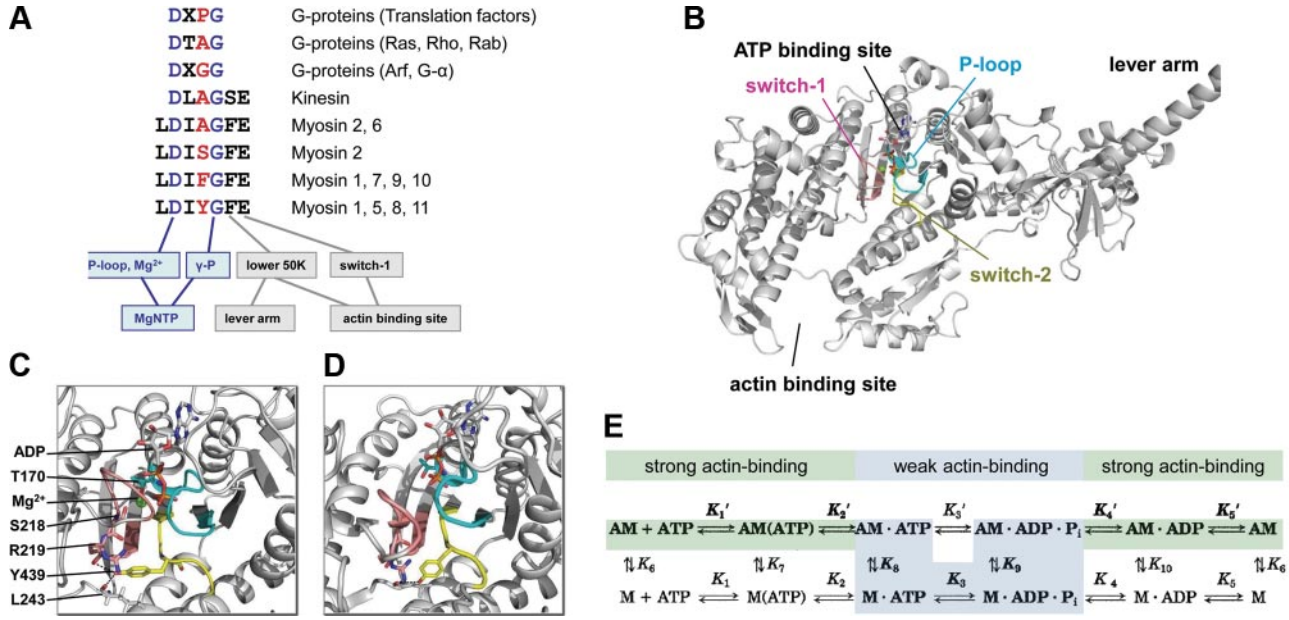

Figure 1. Sequence, location, and roles of switch-2. *A*) Switch-2 amino acid sequence and conserved communication pathways in different NTPases. Residues and pathways conserved in myosins, kinesins, and G proteins are colored blue. Class-specific residue mutated in the current study is highlighted in red. *B*) Location of conserved loops of the ATPase active site within the motor domain of myosin-5a (1W7J). *C*, *D*) Magnified views of the active site in strongly (1W7J, *C*) and weakly (1W7I, *D*) nucleotide-bound states. *E*) Kinetic scheme of the actomyosin ATPase cycle. Nucleotide-free (rigor) actomyosin (AM) binds ATP in two steps (K_1' and K_2'). Myosin head (M) then dissociates (K_8) from actin (A) in the main flux pathway indicated by shading and bold characters. After ATP hydrolysis (K_3), $M \cdot ADP \cdot P_i$ rebinds to actin (K_9), and products are released (P_i in K_4' and ADP in K_5'). Strong and weak actin-binding states are shaded in green and cyan, respectively. All rate and equilibrium constants are defined in the rightward and downward directions.

cessive movement along the actin filament as a two-headed single molecule, which requires the capability to take numerous enzymatic and coupled mechanical steps along the actin filament without detachment (10, 11).

The mechanical output of different myosins is dictated by their biochemical kinetic properties. During the myosin ATPase cycle, the succession of strongly and weakly actin-bound (detached) myosin states is driven by changes in the nucleotide content of the active site (Fig. 1*E*). The kinetic parameters of the steps of the ATPase cycle therefore define the fraction of the cycle time spent by the myosin motor domain in strongly actin-bound states, known as the duty ratio. A high duty ratio (>0.5 for one motor domain) is a prerequisite for processivity of a two-headed single myosin-5a molecule that has to maintain continuous actin attachment during a processive run. The kinetic mechanism of myosin-5a therefore drastically differs from that of the low-duty ratio muscle myosin-2 isoforms (12). The rate-limiting step of the ATPase cycle of myosin-5a is ADP release from actomyosin, which ensures the long lifetime of the strongly bound actomyosin · ADP complex (Fig. 1*E*).

To examine the contribution of the fine tuning of switch-2 structure to the properties of myosin-5a that enable its functioning as an intracellular transporter, we characterized the mechanochemical mechanism of a series of myosin-5a constructs harboring point mutations in the class-specific position of switch-2 (X in the LDIXGFE consensus sequence, position 439 in mouse myosin-5a). Wild-type (wt) myosin-5 has a tyrosine in this position (Fig. 1*A*). The Y439A and Y439S mutants mimic the sequence of wt myosin-2 isoforms. Besides wt myosin-5a and myosin-2 isoforms, crystal structures are also available for myosin-2 mutants harboring a tyrosine or a glutamate in the position homologous to Y439 of myosin-5a [S456Y (PDB codes 1W9I and 1W9J) and S456E *Dictyostelium* myosin-2 (1W9K and 1W9L)]. Therefore, we also created and characterized the Y439E mutant to relate the mutation-induced kinetic changes to structural properties. Our results demonstrate that Y439 enables myosin-5a to step along actin filament in a rapid and processive manner by facilitating actin-activated Mg^{2+}-dependent ADP release.

MATERIALS AND METHODS

Cloning, expression, and protein purification

cDNA coding for the N-terminal 820-aa segment of mouse myosin-5a (m5aS1, comprising the motor domain and the first two IQ motifs), cloned into pFastBac1 baculovirus transfer vector, was used to produce point mutants *via* the QuikChange mutagenesis protocol (Stratagene, La Jolla, CA, USA) using complementary oligonucleotide pairs with coding-strand sequences of CATCGGCGTGCTGGACATCGCCGGATTTGAAACATTTG (for Y439A), CATCGGCGTGCTGGACATCAGCGGATTTGAAACATTTG (for Y439S), and CATCGGCGTGCTGGACATCGAGGGATTTGAAACATTTG (for Y439E; mutant triplets are underscored). The DNA construct coding for wt m5aHMM [coding for an N-terminal green fluorescent protein

(GFP), the first 1091 aa of the heavy chain, comprising the motor domain, all 6 IQ motifs plus the N-terminal segment of the coiled-coil tail] was constructed as described earlier (13). To obtain the plasmid for Y439A-m5aHMM, the mutation was introduced into this construct as described above for Y439A-m5aS1. All DNA constructs were verified by DNA sequencing. Sf9 cells were cotransfected with baculoviruses encoding the myosin heavy-chain fragments and *Xenopus* calmodulin (CaM). Expressed myosin heavy chains contained a C-terminal FLAG-tag to aid purification. Proteins were expressed and purified as described in ref. 14.

Kinetic experiments

Unless stated otherwise, all experiments were performed at 25°C in a buffer comprising 20 mM HEPES (pH 7.0), 50 mM KCl, 5 mM $MgCl_2$, 0.1 mM EGTA, and 1 mM DTT. Steady-state ATPase activities were measured using an NADH-coupled assay (15, 16) at 1 mM ATP if not stated otherwise. Stopped-flow experiments were performed in KinTek SF-2004 (KinTek, Austin, TX, USA) and BioLogic SFM 300 apparatuses (BioLogic, Claix, France). Optical setups were as described earlier (16). Quenched-flow experiments were performed in a KinTek RQF-3 instrument. In all transient kinetic experiments, the volume mixing ratio was 1:1 and postmix concentrations are stated unless otherwise indicated. Actin filaments were stabilized by a 1.5-fold molar excess of phalloidin (Calbiochem, San Diego, CA, USA). In transient kinetic experiments using nucleotide-free m5aS1, nucleotide contamination was removed by preincubation of m5aS1 with 0.02 U/ml apyrase (Sigma-Aldrich, St. Louis, MO, USA) for 15 min at 25°C. P_i release experiments were performed in the presence of a "P_i mop" described in ref. 17. SF-2004 and BioKine instrument software, OriginLab 7.5 (http://www.originlab.com), and Gepasi 3.0 (http://www.gepasi.org) were used for data analysis. In the experiments of Fig. 5*A*, free Mg^{2+} concentrations were calculated using the Maxchelator software (http://www.stanford.edu/~cpatton/MgATP-NIST.htm).

In vitro motility and single-molecule experiments

In vitro actin gliding assays using m5aHMM constructs were performed as described in ref. 18 in a buffer containing 40 mM KCl, 20 mM MOPS (pH 7.5), 5 mM $MgCl_2$, 0.1 mM EGTA, 50 mM DTT, 1 mM ATP, and an oxygen scavenging system consisting of 25 mg/ml glucose, 0.1 mg/ml glucose oxidase, and 2 μg/ml catalase. Actin filaments were labeled with rhodamine-phalloidin. The velocity of individual actin filaments from images was calculated using the Track Objects function of MetaMorph software (Molecular Devices Corp., Sunnyvale, CA, USA). Single-molecule m5aHMM motility assays using total internal reflection fluorescence (TIRF) microscopy were performed as described previously (19). Irradiation (488 nm) from an argon laser was used to excite GFP molecules fused to the N terminus of m5aHMM. Velocities of single molecules were determined from the movement of the fluorophore using MetaMorph software. All experiments were performed at 25°C controlled by an enclose box on an Olympus IX70 microscope (Olympus, Tokyo, Japan) (14).

Structural modeling

Crystal structures of myosin-5a in the postrigor (1W7J) and weak ADP states (1W7I) (20) were used in the study. To model the strong ADP state, energy minimization was performed on removal of BeF_x from 1W7J. The derived model as well as the Y439A models of both strong and weak ADP states were subjected to semiempirical quantum mechanical geometry optimization. Energy minimization was performed using MOE (Molecular Operating Environment suite; Chemical Computing Group Inc., Montreal, QC, Canada) software with AMBER99 force field (21) implemented into the package, up to a root mean square deviation (RMSD) gradient of 0.001 to remove geometric strains. ADP and surrounding amino acid residues within 4 Å were kept rigid during optimization with AMBER99 and then geometry-optimized using the AM1 semiempirical quantum chemical method (22). The RHF-AM1 calculation was halted when the gradient dropped to <0.01. The Yale Morph Server (23) was used for calculating the minimized structural trajectory of the strong-to-weak ADP transition. The Mg^{2+} translation vector during the transition was estimated based on the average translation vectors of the coordinating oxygen atoms of T170 and S218. Local geometry alignments were performed with ProFit software (A. C. R. Martin and C. T. Porter, http://www.bioinf.org.uk/software/profit) defining the switch-1, switch-2, and P-loop regions for fitting.

RESULTS

Protein constructs

In this study we used single-headed [m5aS1 (subfragment-1-like), containing the motor domain and the first two IQ motifs, each binding a calmodulin molecule] and double-headed [m5aHMM (heavy meromyosin-like), containing an N-terminal GFP, the motor domain, all 6 IQ motifs with bound calmodulins, and the proximal part of the coiled-coil tail] constructs of mouse myosin-5a. Wild-type mouse m5aS1 exhibited slightly different kinetic properties from those of the previously characterized chicken m5aS1 (see Discussion and **Table 1**) (12, 24, 25). Nomenclature of all kinetic constants refers to Fig. 1*E*.

Y439 mutations do not impair nucleotide binding, ATP hydrolysis, and phosphate release

We followed the binding of ATP (K_1k_2) and ADP (k_{-5}) to m5aS1 in stopped-flow transient kinetic experiments monitoring signal changes of fluorescently labeled [3′-methylanthraniloyl-2′-deoxy-(md)] nucleotides on rapid mixing with wt and mutant m5aS1 constructs (**Fig. 2*A***). The mutations did not markedly change the nucleotide binding kinetics, with the exception that Y439A showed faster mdATP binding than the other constructs (Fig. 2*A*, Table 1).

We monitored the ATP-induced dissociation of the acto-m5aS1 complex by following the fluorescence increase of pyrene-labeled actin on mixing pyrene-acto-S1 with ATP in the stopped-flow apparatus. The fitted observed rate constants (k_{obs}) showed hyperbolic dependence on the ATP concentration (Fig. 2*B*), which indicates a two-step reaction ($K_1'k_2'$) consisting of a second-order binding step (K_1') followed by a structural change (k_2'). Parameters of these steps were quite variable among wt and mutant m5aS1 constructs, but the maximal k_{obs} at saturating ATP concentration (k_2') was $>80\ s^{-1}$ in all cases (Table 1).

All mutants retained the capability to catalyze ATP

TABLE 1. *Kinetic parameters of wt and switch-2 mutant m5aS1 constructs*

Parameter	wt mouse m5aS1	Y439A	Y439S	Y439E	wt chicken m5aS1
Steady-state parameters					
Basal ATPase activity, k_{cat} (s^{-1})[a]	0.020 ± 0.009	0.086 ± 0.005	0.05 ± 0.01	0.15 ± 0.02	0.03[b]
Actin-activated ATPase activity, k_{cat} (s^{-1})[a]	11 ± 1	1.4 ± 0.1	1.5 ± 0.1	1.0 ± 0.1	15[b]
Actin-activated ATPase activity, K_{actin} (μM)[a]	4.8 ± 0.3	0.36 ± 0.04	0.20 ± 0.08	0.06 ± 0.01	1.4[b]
Trp fluorescence increase on ATP addition (%)[c]	11 ± 3	8 ± 3	22 ± 4	3 ± 1	13[d]
Rate and equilibrium constants in the absence of actin					
ATP binding and hydrolysis					
K_1k_2 (μM^{-1} s^{-1})[c]	1.1	1.2	n.d.	n.d.	1.6[b]
K_1k_2 (μM^{-1} s^{-1})[e]	1.9 ± 0.2	4.1 ± 0.4	1.1 ± 0.1	1.2 ± 0.1	
k_3+k_{-3} (s^{-1})[c]	210 ± 10	250 ± 60	n.d.	n.d.	750[b]
K_3[f]	0.57 ± 0.12	0.52 ± 0.08	1.5 ± 0.5	0.49 ± 0.17	9[d]
Phosphate release					
k_4 (s^{-1})[f]	0.025 ± 0.011	0.42 ± 0.06	0.053 ± 0.038	0.41 ± 0.08	
k_4 (s^{-1})[g]	0.025 ± 0.005	0.34 ± 0.02	0.053 ± 0.006	0.11 ± 0.003	
ADP interaction					
k_5 (s^{-1})[e]	2.5 ± 0.3	2.7 ± 0.3	4.0 ± 0.1	1.6 ± 0.1	1.2[b]
k_{-5} (μM^{-1} s^{-1})[e]	6.9 ± 1.2	5.7 ± 0.5	4.3 ± 0.3	6.2 ± 0.6	4.6[b]
K_5 (= k_5/k_{-5}) (μM)	0.36	0.47	0.93	0.26	0.27[b]
Rate and equilibrium constants in the presence of actin					
ATP binding					
$K_1'k_2'$ (μM^{-1} s^{-1})[h]	1.0 ± 0.1	1.9 ± 0.2	0.43 ± 0.25	0.87 ± 0.16	0.9[b]
k_2' (s^{-1})[h]	210 ± 20	820 ± 80	420 ± 250	94 ± 18	870[b]
Actin binding by M · ADP · P_i and phosphate release					
K_9 (μM)[g]	55 ± 19	3.3 ± 0.9	30 ± 2	47 ± 21	9[i]
k_4' (s^{-1})[g]	240 ± 60	110 ± 10	150 ± 10	210 ± 60	110[i]
ADP interaction					
k_5' (s^{-1})[h]	17 ± 3	3.7 ± 0.3	3.7 ± 0.3	2.1 ± 0.2	16[b]
K_5' (μM)[h]	3.5 ± 1.5	1.8 ± 0.1	<1	<1	0.7[b]
Coupling (K_5'/K_5)	9.7	3.8	<1.1	<3.8	2.6[b]
Acceleration (k_5'/k_5)	6.9	1.4	0.9	1.3	13[b]
Actin interaction					
k_6 (s^{-1})[h]	1.1×10^{-3}	7.6×10^{-3}	2.5×10^{-3}	3.0×10^{-3}	3.6×10^{-4}[b]
k_{-6} (μM^{-1} s^{-1})[h]	28 ± 1	25 ± 6	25 ± 2	24 ± 5	73[b]
K_6 (=k_6/k_{-6}) (μM)	3.9×10^{-5}	3.0×10^{-4}	1.0×10^{-4}	1.3×10^{-4}	4.9×10^{-6}[b]
$\Delta H^{\ddagger}$ (k_6) (kJ/mol)[h]	19 ± 1	38 ± 3	32 ± 1	30 ± 2	

Means ± SE for n = 2–4 are listed. Nomenclature of constants refers to Fig. 1*E*. Conditions: 25°C, 20 mM HEPES (pH 7.0), 50 mM KCl, 5 mM $MgCl_2$, 0.1 mM EGTA, and 1 mM DTT. n.d., not determined. [a]NADH-coupled assay. [b]Data from ref. 12. [c]Tryptophan fluorescence. [d]Data from ref. 24. [e]Deoxymant-nucleotide fluorescence. [f]Quenched-flow. [g]MDCC-PBP fluorescence. [h]Pyrene-actin fluorescence. [i]Data from ref. 25.

hydrolysis. Indeed, their basal (actin-free) steady-state ATPase activities were higher than that of wt m5aS1 (Table 1). On interaction with ATP, the constructs showed an increase in tryptophan fluorescence, probably originating from the ATP-sensitive tryptophan (W483) located in the relay loop at the base of the lever arm (12, 26). This fluorescence increase has been shown to report the reversible transition of switch-2 from an open to a closed conformation (24, 27, 28). ATP hydrolysis occurs only in the switch-2 closed state (28, 29). After ATP hydrolysis, switch-2 probably needs to reopen for phosphate (P_i) release in the absence of actin, which is rate-limiting in the basal (actin-free) ATPase cycle (29, 30). Consistent with this model, we found that a smaller increase in tryptophan fluorescence was accompanied by higher basal ATPase activity in the Y439A and Y439E mutants (Table 1). On mixing wt and Y439A-m5aS1 with ATP in the stopped-flow apparatus, k_{obs} of the tryptophan fluorescence increase showed a hyperbolic dependence on ATP concentration (Fig. 2*C*, inset). The maximal k_{obs}, reporting the kinetics of ATP hydrolysis (k_3+k_{-3}) (12), was >100 s^{-1} in both constructs (Table 1).

In single-turnover quenched-flow experiments, the time course of ATP hydrolysis was biphasic in all constructs, with the rapid phase being rate-limited by ATP binding and the slow phase by phosphate (P_i) release (*cf.* P_i release experiments below) (Fig. 2*C*). Analysis of the fractional amplitudes showed that the mutations did not markedly change the equilibrium constant of the ATP hydrolysis step (Fig. 2*C*; Table 1).

We measured the kinetics of P_i release from M · ADP · P_i (k_4) and AM · ADP · P_i (K_9, k_4') in double-mixing single-turnover stopped-flow experiments using the signal of a fluorescently labeled bacterial phosphate bind-

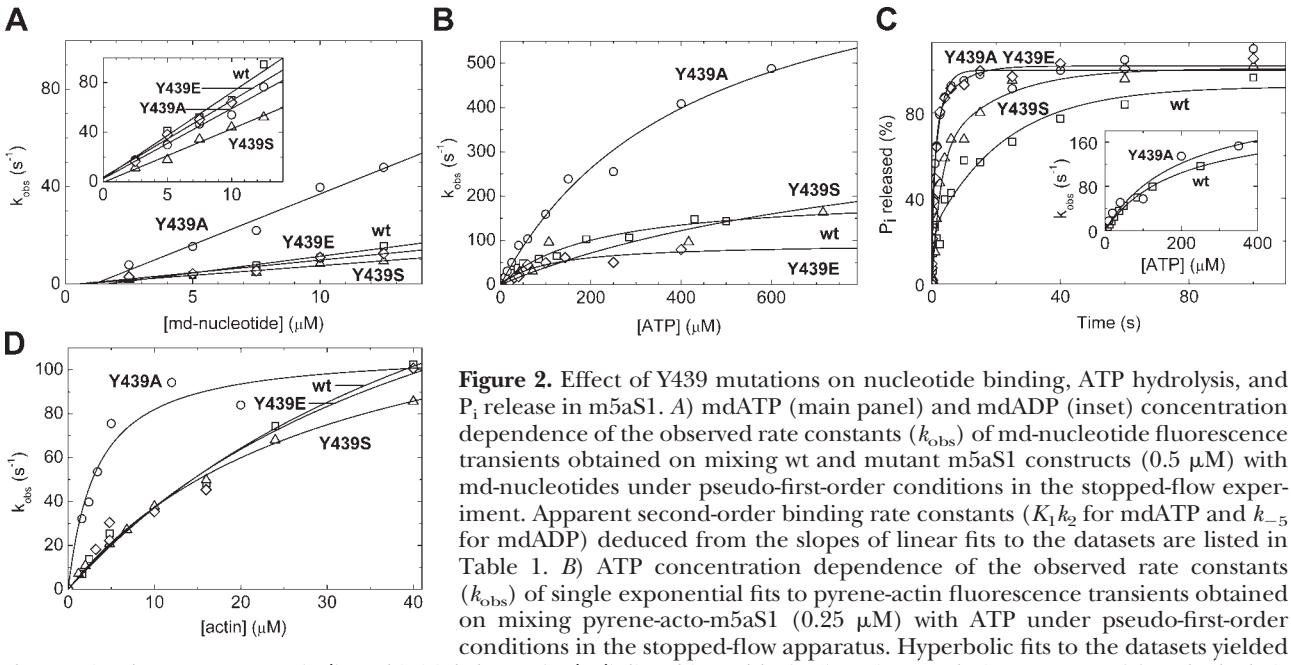

Figure 2. Effect of Y439 mutations on nucleotide binding, ATP hydrolysis, and P_i release in m5aS1. *A*) mdATP (main panel) and mdADP (inset) concentration dependence of the observed rate constants (k_{obs}) of md-nucleotide fluorescence transients obtained on mixing wt and mutant m5aS1 constructs (0.5 μM) with md-nucleotides under pseudo-first-order conditions in the stopped-flow experiment. Apparent second-order binding rate constants (K_1k_2 for mdATP and k_{-5} for mdADP) deduced from the slopes of linear fits to the datasets are listed in Table 1. *B*) ATP concentration dependence of the observed rate constants (k_{obs}) of single exponential fits to pyrene-actin fluorescence transients obtained on mixing pyrene-acto-m5aS1 (0.25 μM) with ATP under pseudo-first-order conditions in the stopped-flow apparatus. Hyperbolic fits to the datasets yielded the maximal rate constants (k_2') and initial slopes ($K_1'k_2'$) listed in Table 1. *C*) Main panel, time course of ATP hydrolysis on mixing 3.5 μM m5aS1 with 2 μM ATP (single turnover conditions) in the quenched-flow experiment, fitted by double exponential approximations. The equilibrium constant of the ATP hydrolysis step (K_3) and the rate constant of P_i release (k_4) were calculated from the fractional amplitude of the rapid phase [F_1; $K_3=F_1/(1-F_1)$] and the k_{obs} of the slow phase ($k_{obs,\,2}=k_4$), respectively (Table 1). Inset: ATP concentration dependence of the single exponential k_{obs} of tryptophan fluorescence increase on mixing m5aS1 (0.5 μM) with ATP under pseudo-first-order conditions in the stopped-flow experiment. Initial slopes (K_1k_2) and maximal k_{obs} values (k_3+k_{-3}) obtained from hyperbolic fits to the datasets are listed in Table 1. *D*) Actin concentration dependence of the k_{obs} of P_i release from m5S1 · ADP · P_i and acto-m5aS1 · ADP · P_i, measured in double-mixing stopped-flow experiments monitoring MDCC-PBP fluorescence (3 μM in all syringes). First, 0.7 μM m5aS1 was rapidly mixed with 0.3 μM ATP (single turnover; concentrations after first mix), incubated for 3 s to let ATP binding and hydrolysis occur, and then rapidly mixed with increasing concentrations of actin (postmix concentrations shown). Hyperbolic fits to the datasets yielded the maximal k_{obs} (k_4') and half-saturating actin concentration (K_9) values listed in Table 1. □, wt m5aS1; ○, Y439A; △, Y439S; ◇, Y439E. Conditions were as in Table 1.

ing protein (MDCC-PBP) (17). k_{obs} values obtained in the absence of actin (k_4) were close to the basal ATPase activities of the constructs, showing that P_i release is rate-limiting in all mutants (Table 1). k_{obs} showed a hyperbolic dependence on actin concentration, delineating maximal actin-activated P_i release rate constants (k_4') >100 s^{-1} in all constructs (Fig. 2*D*; Table 1). In the presence of actin, an additional slow P_i release phase was present, which was earlier attributed to actin-attached ATP hydrolysis in myosin-2 (31).

Taken together, the above results show that although the Y439 mutations detectably affect nucleotide binding, ATP hydrolysis, and P_i release, these processes all remain rapid and not rate-limiting in the actin-activated ATPase cycle of the mutants, similarly to the wt (see also below).

Y439 mutations abolish actin-activation of ADP release

We determined the ADP affinity of actomyosin ($1/K_5'$) by following the time course of ATP-induced dissociation of pyrene-acto-S1 preincubated with different ADP concentrations. In the biphasic transients obtained, the rapid phase originated from ATP-induced dissociation of ADP-free actomyosin, whereas the slow phase represented the ADP-bound fraction of acto-S1, in which the slow dissociation of ADP limited the rate of the oncoming ATP-induced acto-S1 dissociation. Analysis of the fractional amplitudes indicated that all mutants exhibited a higher ADP affinity in the actin-bound state than wt m5aS1 (**Fig. 3*A***; Table 1). Correspondingly, the rate constant of ADP dissociation (k_5') was ~5 times slower in the mutants than in wt m5aS1 (Fig. 3*B*; Table 1).

ADP release from actomyosin (k_5') is the rate-limiting step of the actin-activated ATPase cycle of myosin-5a (12). We found that the maximal actin-activated ATPase activities of all m5aS1 constructs were close to the ADP release rate constants, indicating that the mutants retained ADP release as the rate-limiting step (Fig. 3*B, C*; Table 1).

Comparison of the ADP release constants of acto-m5aS1 (k_5') with those obtained in the absence of actin (in mdADP chasing experiments, k_5 in Table 1) reveals that, although actin significantly accelerates ADP release from wt m5aS1, there is practically no acceleration in the mutants (k_5'/k_5 in Table 1). Correspondingly, the thermodynamic coupling between actin and ADP binding to m5aS1 (*i.e.*, the ratio of ADP-binding K_d values in the presence and absence of actin, K_5'/K_5) is lower in the mutants (Table 1).

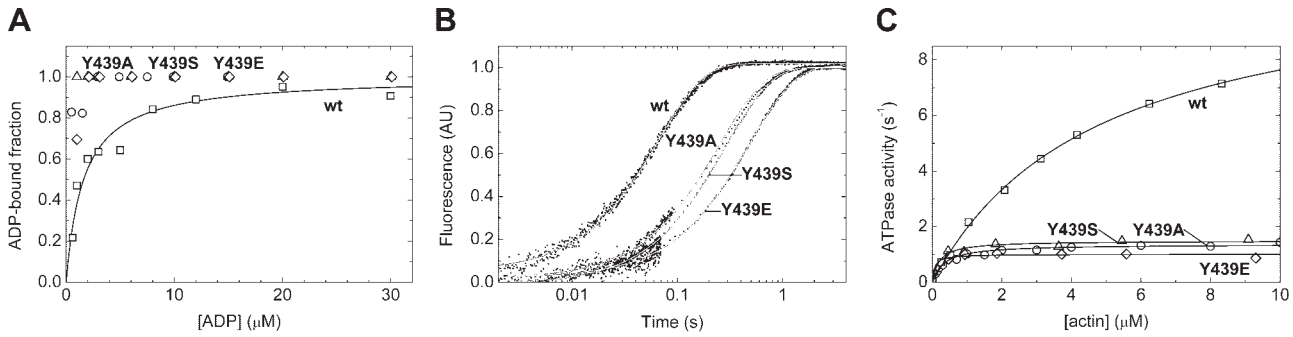

Figure 3. Effect of Y439 mutations on the ADP interaction and ATPase activity of m5aS1. *A*) ADP concentration dependence of the fractional saturation of acto-m5aS1 by ADP, as monitored from the fractional amplitudes of biphasic pyrene-actin fluorescence stopped-flow transients obtained on mixing acto-m5aS1 (0.2 μM) plus ADP (indicated premix concentrations) with 200 μM ATP. Hyperbolic fit to the fractional amplitude of the slow phase (representing the ADP-bound fraction of pyrene-acto-m5aS1) yielded a K_5' of 3.5 μM for wt m5aS1, whereas the datasets for the mutants indicated K_5' values below 2 μM (Table 1). k_5' values reported in Table 1 are averages of k_{obs} of the slow phase of transients at different ADP concentrations. *B*) Pyrene-actin fluorescence traces obtained on rapidly mixing the preincubated complex of pyrene-acto-m5aS1 (0.2 μM) and ADP (20 μM) with 200 μM ATP in the stopped-flow apparatus. ADP release from acto-m5aS1 · ADP is rate-limiting in these conditions. Fitted single-exponential k_{obs} (k_5') values of the traces shown were 20 s^{-1} (wt m5aS1), 3.4 s^{-1} (Y439A), 3.3 s^{-1} (Y439S), and 1.9 s^{-1} (Y439E). *C*) Dependence of the steady-state actin-activated ATPase activity of m5aS1 on actin concentration. Hyperbolic fits to the datasets yielded the maximal ATPase activities (k_{cat}) and half-saturating actin concentrations (K_{actin}) listed in Table 1. Symbols are as in Fig. 2. Conditions were as in Table 1. AU, arbitrary units.

Y439A mutation slows down processive translocation

ADP release from actomyosin gates the exit of myosin-5a heads from the strong actin-binding state, and, thus, it is thought to be rate-limiting for translocation along actin filaments (6). We conducted *in vitro* actin gliding and TIRF microscopy-based single-molecule motility assays using GFP-labeled wt and Y439A-m5aHMM constructs to determine translocation speed and processivity. In both types of assay, the speed of Y439A-m5aHMM was decreased compared with the wt (**Fig. 4*A*, *B***), by exactly the same factor (4.5) as in the case of ADP release from actomyosin in the transient kinetic experiments of Fig. 3*A*, *B*. These results demonstrate that, similarly to the wt enzyme, ADP release from actomyosin remains rate-limiting in the Y439A mutant in both actin-activated ATPase activity (Fig. 3*C*) and translocation along actin filaments (Fig. 4*A, B*). Importantly, our single-molecule motility experiments also showed that Y439A-m5aHMM is capable of performing processive runs on actin with run lengths similar to those of the wt construct (~1 μm at 1 mM ATP) (Fig. 4*C*).

Y439A mutation abolishes actin-activation of ADP release in a Mg^{2+}-controlled manner

It has been shown in kinetic and structural studies that the release of MgADP from myosin-5a and actomyosin-5a is controlled through the release of the Mg^{2+} ion (20, 32, 33). Therefore, we measured the effect of Mg^{2+} on both the steady-state actin-activated ATPase activity and the transient kinetics of ADP release from wt and Y439A-m5aS1. The steady-state acto-m5aS1 ATPase ac-

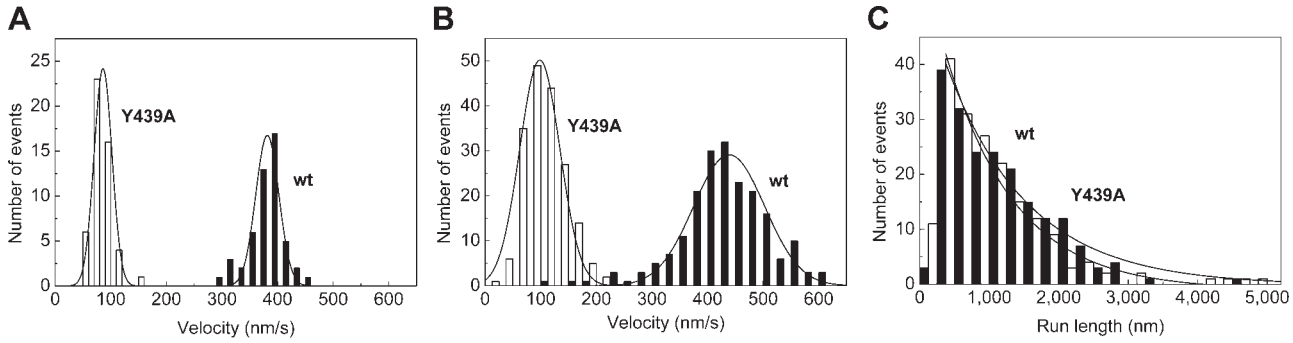

Figure 4. Effect of the Y439A mutation on the translocation speed and processivity of m5aHMM. *A*) The *in vitro* actin gliding speed of wt (solid columns) and Y439A-m5aHMM (open columns) was 380 ± 30 nm/s and 86 ± 31 nm/s, respectively. *B*) In single-molecule TIRF assays, the translocation speed of single m5aHMM molecules (440±120 nm/s for wt and 98±72 nm/s for Y439A) was similar to that of actin gliding (*A*). *C*) Run length distribution of wt (■) and Y439A-m5aHMM (□) in single-molecule TIRF motility assays. Single exponential fits to the datasets yielded mean run lengths of 1300 ± 100 nm (upper line) and 1000 ± 100 nm (lower line) for wt and Y439A, respectively. Errors indicate gaussian half-widths in *A* and *B* and fitting SE in *C*. Data points < 250 nm were omitted from the fits in *C*. Conditions were as described in Materials and Methods.

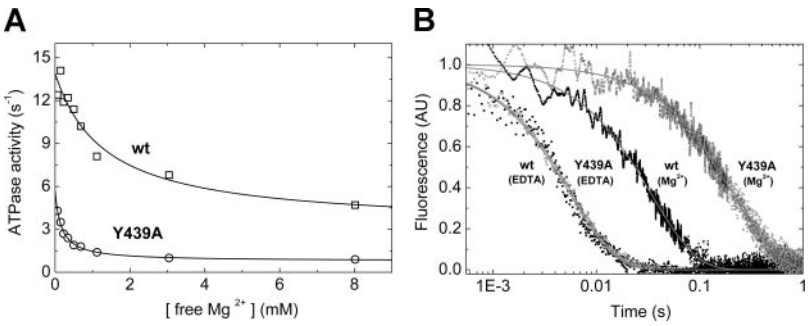

Figure 5. Effect of Mg^{2+} on the ATPase activity of and ADP release from acto-wt-m5aS1 and acto-Y439A-m5aS1. *A*) Inhibition of the ATPase activity of wt (□) and Y439A (○) acto-m5aS1 by free Mg^{2+}. Hyperbolic fits to the datasets showed that the ATPase activity of acto-wt-m5aS1 dropped from 14 ± 0.7 s^{-1} (at 0 free Mg^{2+} concentration) to 3.2 ± 1.2 s^{-1} (at saturating Mg^{2+}) with half-maximal effect at 1.3 ± 0.6 mM Mg^{2+}. The ATPase activity of acto-Y439A-m5aS1 dropped from 5.7 ± 0.3 to 0.8 ± 0.2 s^{-1} with half-maximal effect at 0.16 ± 0.02 mM Mg^{2+}. Concentrations applied were 0.1 μM m5aS1, 10 μM actin, 2 mM ATP, and various $MgCl_2$ concentrations to yield the indicated free Mg^{2+} concentrations. *B*) mdADP fluorescence transients obtained on mixing the acto-m5aS1 · mdADP complex (0.5 μM wt (■) or Y439A (○) m5aS1, 5 μM actin, and 25 μM mdADP) with 500 μM ATP in the stopped-flow in the presence of 1 mM EDTA or 5 mM $MgCl_2$ (in both syringes). Single exponential fits to the transients shown yielded k_{obs} values of 180 s^{-1} (wt, EDTA), 29 s^{-1} (wt, Mg^{2+}), 170 s^{-1} (Y439A, EDTA), and 4.8 s^{-1} (Y439, Mg^{2+}). See Table 2 for a summary of mdADP release rate constants obtained. Other conditions were as in Table 1.

tivity was markedly inhibited by the presence of free Mg^{2+} ions, both in wt and Y439A-m5aHMM (**Fig. 5*A***). We monitored the release of mdADP from m5aS1 and acto-m5aS1 (wt and Y439A constructs) both in the absence and presence of 5 mM Mg^{2+} in transient kinetic experiments in which excess ATP was used as a chaser (Fig. 5*B*; **Table 2**). The mdADP release rate constants summarized in Table 2 show that the effect of the Y439A mutation on mdADP release from m5aS1 is specific for the presence of both actin and Mg^{2+}, and thus the mutation abolishes actin activation of ADP release from m5aS1 in a Mg^{2+}-controlled manner. Our results for wt m5aS1 are in agreement with earlier studies on wt chicken m5aS1 (Fig. 5*B*; Table 2) (32, 33).

Y439 influences MgADP release through interaction with switch-1

To explain the role of Y439 in Mg^{2+}-dependent ADP release, the interactions of Y439 were analyzed at the atomic level. Atomic structures of myosin-5a with bound MgADP · BeF_x (PDB code: 1W7J) and with Mg^{2+}-free ADP (1W7I) have been determined (20). Although the 1W7J structure contains an ATP analog, it has been shown in various myosins that this state is structurally equivalent to a strongly MgADP-bound state (called postrigor) (29), whereas the 1W7I structure has been proposed to represent a "weak ADP" state in which Mg^{2+} release has taken place (20). The postrigor state is adopted by myosin in solution in the presence of ADP and various ATP analogs, and it is thought to occur in the working cycle after the ATP-induced dissociation of actomyosin (4). Although this structure represents an actin-detached state, some of its features may resemble those of the actomyosin · ADP state from which ADP is released during the rate-limiting step of the mechanochemical cycle of processive myosins. In the postrigor state, Y439 forms hydrogen bonds with the backbone carbonyl of the conserved L243 and also that of R219 of switch-1 (Fig. 1*C*). The latter interaction disappears in the weak ADP state (Fig. 1*D*), and thus the Y439-R219 hydrogen bond seems to contribute to the coupling of switch-1 and switch-2 movements occurring on Mg^{2+} release. A conformational change is associated with the disappearance of the Y439-R219 hydrogen bond, which also affects the conformation of the neighboring Mg^{2+}-coordinating S218 of switch-1.

TABLE 2. *Mg^{2+}-dependent mdADP release in wt and Y439A-m5aS1*

	Rate constant (s^{-1})	
Genotype	1 mM EDTA	5 mM Mg^{2+}
wt (− actin)	43 ± 15	2.5 ± 0.3
wt (+ actin)	160 ± 20	23 ± 4
Y439A (− actin)	55 ± 20	2.7 ± 0.3
Y439A (+ actin)	170 ± 20	3.3 ± 0.6

mdADP release rate constants were determined as shown in Fig. 5*B*. Means ± SE for n = 3–5 are listed. Conditions were as in Table 1, except that 1 mM EDTA was used instead of 5 mM $MgCl_2$ where indicated.

To investigate the conformational changes during the transition from strong MgADP (postrigor) to the Mg^{2+}-free weak ADP state, we produced an energy-minimized strong MgADP state by removing BeF_x from the 1W7J structure. This structure remained very similar to 1W7J (RMSD=0.72 Å). Intermediate coordinates for the trajectory between the strong MgADP and weak ADP states were calculated with the help of the Yale Morph Server (Supplemental Movie 1). The calculation revealed that in the amino acid residues within 4 Å of Y439 the side chain conformations remained unchanged during the transition from strong ADP to weak ADP state. In contrast, Y439 has undergone a large conformational change during the transition. To quantitatively analyze the conformational changes of the individual amino acid residues, RMSD values between strong and weak ADP conformations were calculated (Supplemental Fig. 1). To exclude the translational movement of the backbone of the whole region, which would lead to nonspecific overestimation of the RMSD, local alignment and by-residue RMSD calculation was

performed based on the relevant regions of the protein (switch-1, switch-2, and P-loop) rather than on the protein as whole. The greatest RMSD was observed for Y439 and F441 of switch-2, whereas no significant changes were observed in the core region of the P-loop (G163-T170) and switch-1 (N214-G221) (Supplemental Fig. 1). F441 has been shown be important in the coupling between switch-2 and the actin-binding cleft through the L50 subdomain (34), which suggests a structural pathway to explain our experimental finding that the actin activation of ADP release is abolished in the absence of Y439 (Fig. 3*B*; Tables 1 and 2).

The Y439A mutation did not significantly influence the protein structures on energy minimization: RMSD values of 0.76 and 0.80 Å between wt and Y439A were observed in strong MgADP and weak ADP states, respectively. Naturally, the above described communication pathway between switch-1 and switch-2 of wt-m5aS1 was absent in the mutant.

Y439 mutations influence the energetics of actin binding

The bulky tyrosine residue in this position has been shown to cause a specific switch-2 conformation in the rigor-like (nucleotide-free, actin-bound) state of myosin-5 (35). Therefore, we investigated the effect of Y439 mutations on the interaction of nucleotide-free m5aS1 with actin. We determined the second-order actin-binding rate constant of nucleotide-free m5aS1 (k_{-6}) from the slopes of the pyrene-actin concentration dependence of the k_{obs} of pyrene-actin fluorescence transients recorded on rapidly mixing of m5aS1 with excess pyrene-actin under pseudo-first-order conditions in the stopped-flow apparatus. The rate constant of dissociation of nucleotide-free m5aS1 from actin (k_6) was measured in chasing experiments in which pyrene-acto-m5aS1 was mixed with excess unlabeled actin. The mutations caused small differences in the binding and dissociation rate constants, resulting in slightly reduced actin affinities ($1/K_6$) compared with wt m5aS1 (Table 1). The temperature dependence of actin binding (k_{-6}) was markedly higher in the mutants than in wt m5aS1, indicating that the mutations caused a significant increase in the activation enthalpy ($\Delta H^{\ddagger}$) of actin binding (Supplemental Fig. 2; Table 1).

DISCUSSION

Structural adaptation of switch-2 for rapid processive motility

The class-specific variation of a central position (Y439 in myosin-5a) of the conserved switch-2 loop of the ATPase active site is an intriguing feature of myosins and other NTPases. Myosins from classes 6 and 7 and some (but not all) myosin-5 isoforms have been shown to be processive (10, 36–40). The nature of the amino acid occupying the Y439-equivalent position does not seem to simply correlate with the processivity of different myosins (Fig. 1*A*) and is indeed reflected in our finding that the replacement of Y439 of myosin-5a with residues with smaller side chains (A or S) found in myosin-2 isoforms did not convert myosin-5a into a low-duty ratio, muscle myosin-2-like motor. In contrast, the most important functional consequence of the mutations was that they decreased the speed of processive translocation of myosin-5a by abolishing the actin-induced acceleration of ADP release (Figs. 3*B, C*; 4*A*, *B*; and 5; Tables 1 and 2). Interestingly, actin does not accelerate ADP release from myosin-6 that harbors an alanine in the Y439-equivalent position (Fig. 1*A*) (41). Thus, the class-specific switch-2 structure of myosin-5 seems to reflect an adaptation to more rapid translocation along actin filaments. The slowing of ADP release from actomyosin (and thus the exit from the strong actin-binding states) in Y439A compared with wt myosin-5a did not increase its processivity, most likely because of a parallel reduction in the maximal rate constant of P_i release from the actomyosin · ADP · P_i complex (k_5' and k_4' in Table 1). Estimates for the single-head duty ratio, calculated as $k_5'/(k_5'+k_4')$, yield high values for both wt and Y439A (0.94 and 0.97, respectively; note that these estimates contain considerable error due to uncertainties in rate constant values).

Effect of alterations of switch-2 structure on Mg^{2+} and nucleotide interaction

Atomic structures of wt and switch-2 mutant *Dictyostelium* myosin-2 (Ddm2) motor domains in the post-trigor conformation show structural alterations caused by the introduction of Y439 in place of the wt serine residue (myosin-5a numbering is applied for all isoforms throughout this article). The C-terminal part of switch-2 (G440-E442), especially the side chain of F441, adopts a different conformation in the post-trigor structure of wt Ddm2 (PDB code 1MMD) compared with m5aS1 (1W7J). Interestingly, the S439Y, but not the S439E, mutation in Ddm2 (1W9I and 1W9K, respectively) induces a myosin-5a-like switch-2 and F441 conformation. At the same time, F441, the key link to the lower 50-kDa subdomain and the actin-binding cleft, shows the largest RMSD (besides Y439) on the strong-to-weak ADP transition (see Results).

A striking feature of the Y439A mutant of myosin-5a is the more pronounced Mg^{2+}-dependent suppression of ADP release from actomyosin compared with the wt (Fig. 5*B*; Table 2). Rosenfeld *et al.* (33) suggested that, in wt myosin-5a, the actin-induced acceleration of ADP release is due to the abolishment of the coordination of Mg^{2+} by the P-loop and other elements of the ATP-binding site. Our results are consistent with this model as the abolishment of the actin-activation of ADP release in Y439A-m5aS1 is controlled by Mg^{2+} release (Fig. 5*B*; Table 2), probably due to altered coordination of the cation. Coureux *et al.* (20) proposed that, during force generation, the release of P_i from actomyosin ·

ADP · P_i first leads to a strong ADP-binding actomyosin · ADP state and, accompanied by the loss of Mg^{2+} from the active site, this state reversibly proceeds to a weak ADP-binding state from which ADP is released. (The simplified scheme in Fig. 1*E* lumps these states into a single AM · ADP state.) Based on this model, the strengthening of the free Mg^{2+}-dependent suppression of ADP release from actomyosin in the Y439A myosin-5a mutant indicates that Y439 in wt myosin-5a contributes to relatively rapid ADP release and thus enhances the speed of processive translocation *via* promotion of the weak ADP-binding conformation (Fig. 5; Table 2; Supplemental Movie 1).

The presence of tyrosine in the Y439-equivalent position of *Dictyostelium* myosins 1D and 1E is linked to significant dependence of ADP release and *in vitro* motility on free Mg^{2+} concentration, in contrast to *Dictyostelium* myosin-1B harboring phenylalanine at this position and being Mg-independent (42–44). These results suggest that the interactions of the Y439 hydroxyl may be important for controlling Mg^{2+}-dependent ADP release in myosin-1. Interestingly, our results show that the Y439A mutation in myosin-5a causes even more pronounced Mg^{2+} sensitivity of ADP release than that in the wt (Fig. 5*B*, Table 2). These findings indicate that the presence of Y439 has a influence on Mg^{2+} coordination in myosin-5a different from that in myosin-1.

Even though the kinetic parameters of ATP binding, ATP-induced actomyosin dissociation, ATP hydrolysis, and P_i release were detectably affected by the mutations (all of these steps were significantly accelerated by the Y439A mutation) (Fig. 2; Table 1), these changes only moderately affect the overall steady-state parameters of m5aS1. The intact capability of the mutants to bind and hydrolyze ATP is in line with the finding that the active-site loops adopt identical conformations in wt, S439Y, and S439E Ddm2 structures in the hydrolysis-competent prepowerstroke state (PDB codes 1MND, 1W9J and 1W9L, respectively). The mutation-induced changes in ATP-induced Trp fluorescence enhancement of m5aS1 reflect changes in the equilibrium between postrigor and prepowerstroke states that precedes the ATP hydrolysis step (Table 1) (28, 45). (The simplified scheme in Fig. 1*E* depicts the conformational equilibrium and ATP hydrolysis as a single K_3 step.) These changes are probably due to the influence of mutations on the postrigor rather than on the prepowerstroke conformation (see above). Interestingly, introduction of an S439L substitution into Ddm2 had a drastic effect on the step size and motility, probably through influencing the prepowerstroke state structure (46). On the other hand, the S439A substitution did not have any significant effect on Ddm2 ATPase activity and motility (34).

Effect of switch-2 structure on actin binding

Contrary to many other myosins, in the absence of actin and nucleotides myosin-5a has been shown to adopt a rigor-like structure characterized by a closed actin binding cleft and rapid, temperature-insensitive (small activation-enthalpy) actin binding (12, 35). In the myosin-5a rigor-like structure, switch-2 showed a uniquely close association with strand 4 of the central β-sheet, which was postulated as a hallmark of the rigor-like state (35). This association was later shown to be absent in rigor-like structures of muscle myosin-2 isoforms in which switch-2 adopts a different conformation (47), and thus it seems to be a specific feature of myosin-5a. Nevertheless, here we show that the removal of the bulky side chain of Y439 from switch-2 of myosin-5a increases the temperature dependence (and the activation enthalpy) of rigor actin binding in proportion to the size of the substituent side chain and reduces the actin affinity in the absence of nucleotides (Supplemental Fig. 2; Table 1). These results suggest that the unique switch-2 conformation of wt myosin-5a, adopted because of the presence of Y439, enables strong and low-energy barrier actin binding *via* facilitating closure of the actin-binding cleft through allosteric effects.

Functional differences between vertebrate myosin-5a orthologs

The present study represents the first detailed kinetic investigation of wt mouse myosin-5a; most of the detailed kinetic and structural investigations on myosin-5a have been performed using the chicken isoform (Table 1) (12, 20, 24, 25, 35). The two orthologs share 95% motor domain sequence identity and exhibit similar processive stepping behavior (8, 10, 11, 13, 14, 19). Chicken m5aS1 complexed with CaM showed K_3, $k_3 + k_{-3}$, and K_{actin} values similar to those determined here for mouse m5aS1-CaM, whereas ATP hydrolysis was more rapid (higher k_3+k_{-3}) and favorable (higher K_3), and half-maximal actin activation occurred at a lower actin concentration (K_{actin}) when chicken m5aS1 was complexed with the essential light chain (ELC) generally used for that isoform (48). These findings suggest that the above parameters are more influenced by the identity of the light chain than the origin of the heavy chain. The parallel increase in $k_3 + k_{-3}$ and K_3 in essential light chain-complexed chicken myosin-5a may reflect that fact that a rapid conformational equilibrium between postrigor and prepowerstroke states (see above) (28, 45), which precedes the chemical step of ATP hydrolysis, is more shifted to the hydrolysis-competent prepowerstroke state than in CaM-complexed chicken or mouse myosin-5a. Taken together, the earlier and present results show that all of the myosin-5a heavy chain-light chain complexes investigated retain the key kinetic adaptations required for processivity, whereas the relatively high affinity of the weak actin-binding states and the high equilibrium constant of ATP hydrolysis may not generally prove to be a crucial aspect of processive myosin motility (12, 24, 25). On the other hand, kinetic parameters related to strongly bound actomyosin complexes were not light chain-dependent in chicken myosin-5a (48). Thus, the lower

actin affinity of nucleotide-free myosin (higher K_6), the reduced ADP affinity of acto-myosin (higher K_5'), and the increased actin-ADP coupling (mutual weakening of actin and ADP binding to myosin) in mouse m5aS1, compared with chicken m5aS1, probably represent heavy chain-specific functional differences (Table 1).

CONCLUSIONS

The ability to engineer the speed and/or processivity of myosin-5a translocation using functionally well-characterized point mutations, as demonstrated in the current work and in an earlier study on a myosin-5a switch-1 mutation (49), will enable precise investigations of its physiological role in processes such as the presynaptic activation of photoreceptor cells and the targeting of the endoplasmic reticulum into the dendritic spines of Purkinje cells (50, 51). Besides the nucleotide-dependent actin interaction of myosins, switch-2 appears to play a general role in the allosteric regulation of Mg^{2+}-dependent NDP release in NTPase enzymes. This role has been pointed out in a structural study on the PRONE guanine nucleotide exchange factor (GEF)-activated GDP release from the Rop GTPase (52). Based on a number of studies on G proteins, a general model of GEF catalysis has emerged whereby GEFs enhance GDP release by inducing a Mg^{2+}-free switch-2 conformation with low nucleotide affinity, in a manner that appears analogous to the effect of actin on Mg^{2+}-controlled ADP dissociation from myosins. Allosterically induced MgNDP release from motors and signaling enzymes will continue to be a focus of attention, as an essential and conserved regulatory mechanism controlling a range of biological processes. FJ

This work was supported by the Fogarty International Center and the National Heart, Lung, and Blood Institute (grant 1 R01-TW007241), Hungarian Scientific Research Fund (OTKA) grants K71915 and NNF78783, and a European Molecular Biology Organization-Howard Hughes Medical Institute startup grant to M.K. M.K. is a Bolyai Fellow of the Hungarian Academy of Sciences. The authors declare that they have no competing financial interests.

REFERENCES

1. Kull, F. J., Vale, R. D., and Fletterick, R. J. (1998) The case for a common ancestor: kinesin and myosin motor proteins and G proteins. *J. Muscle Res. Cell Motil.* **19,** 877–886
2. Vale, R. D. (1996) Switches, latches, and amplifiers: common themes of G proteins and molecular motors. *J. Cell Biol.* **135,** 291–302
3. Bourne, H. R., Sanders, D. A., and McCormick, F. (1991) The GTPase superfamily: conserved structure and molecular mechanism. *Nature* **349,** 117–127
4. Geeves, M. A., and Holmes, K. C. (2005) The molecular mechanism of muscle contraction. *Adv. Protein Chem.* **71,** 161–193
5. De La Cruz, E. M., and Ostap, E. M. (2004) Relating biochemistry and function in the myosin superfamily. *Curr. Opin. Cell Biol.* **16,** 61–67
6. Sellers, J. R. (1999) *Myosins*, Oxford University Press, New York
7. Cheney, R. E., O'Shea, M. K., Heuser, J. E., Coelho, M. V., Wolenski, J. S., Espreafico, E. M., Forscher, P., Larson, R. E., and Mooseker, M. S. (1993) Brain myosin-V is a two-headed unconventional myosin with motor activity. *Cell* **75,** 13–23
8. Sellers, J. R., and Veigel, C. (2006) Walking with myosin V. *Curr. Opin. Cell Biol.* **18,** 68–73
9. Sweeney, H. L., and Houdusse, A. (2004) The motor mechanism of myosin V: insights for muscle contraction. *Philos. Trans. R. Soc. Lond. B Biol. Sci.* **359,** 1829–1841
10. Mehta, A. D., Rock, R. S., Rief, M., Spudich, J. A., Mooseker, M. S., and Cheney, R. E. (1999) Myosin-V is a processive actin-based motor. *Nature* **400,** 590–593
11. Veigel, C., Schmitz, S., Wang, F., and Sellers, J. R. (2005) Load-dependent kinetics of myosin-V can explain its high processivity. *Nat. Cell Biol.* **7,** 861–869
12. De La Cruz, E. M., Wells, A. L., Rosenfeld, S. S., Ostap, E. M., and Sweeney, H. L. (1999) The kinetic mechanism of myosin V. *Proc. Natl. Acad. Sci. U. S. A.* **96,** 13726–13731
13. Snyder, G. E., Sakamoto, T., Hammer, J. A., 3rd, Sellers, J. R., and Selvin, P. R. (2004) Nanometer localization of single green fluorescent proteins: evidence that myosin V walks hand-over-hand via telemark configuration. *Biophys. J.* **87,** 1776–1783
14. Sakamoto, T., Wang, F., Schmitz, S., Xu, Y., Xu, Q., Molloy, J. E., Veigel, C., and Sellers, J. R. (2003) Neck length and processivity of myosin V. *J. Biol. Chem.* **278,** 29201–29207
15. Trentham, D. R., Bardsley, R. G., Eccleston, J. F., and Weeds, A. G. (1972) Elementary processes of the magnesium ion-dependent adenosine triphosphatase activity of heavy meromyosin. A transient kinetic approach to the study of kinases and adenosine triphosphatases and a colorimetric inorganic phosphate assay in situ. *Biochem. J.* **126,** 635–644
16. Wang, F., Kovacs, M., Hu, A., Limouze, J., Harvey, E. V., and Sellers, J. R. (2003) Kinetic mechanism of non-muscle myosin IIB: functional adaptations for tension generation and maintenance. *J. Biol. Chem.* **278,** 27439–27448
17. Brune, M., Hunter, J. L., Corrie, J. E., and Webb, M. R. (1994) Direct, real-time measurement of rapid inorganic phosphate release using a novel fluorescent probe and its application to actomyosin subfragment 1 ATPase. *Biochemistry* **33,** 8262–8271
18. Yildiz, A., Forkey, J. N., McKinney, S. A., Ha, T., Goldman, Y. E., and Selvin, P. R. (2003) Myosin V walks hand-over-hand: single fluorophore imaging with 1.5-nm localization. *Science* **300,** 2061–2065
19. Sakamoto, T., Yildez, A., Selvin, P. R., and Sellers, J. R. (2005) Step-size is determined by neck length in myosin V. *Biochemistry* **44,** 16203–16210
20. Coureux, P. D., Sweeney, H. L., and Houdusse, A. (2004) Three myosin V structures delineate essential features of chemo-mechanical transduction. *EMBO J.* **23,** 4527–4537
21. Wang, J., Cieplak, P., and Kollman, P. A. (2000) How well does a restrained electrostatic potential (RESP) model perform in calculating conformational energies of organic and biological molecules. *J. Comput. Chem.* **21,** 1049–1074
22. Dewar, M. J. S., Zoebisch, E. G., Healy, E. F., and Stewart, J. J. P. (1985) AM1: a new general purpose quantum mechanical molecular model. *J. Am. Chem. Soc.* 107
23. Flores, S., Echols, N., Milburn, D., Hespenheide, B., Keating, K., Lu, J., Wells, S., Yu, E. Z., Thorpe, M., and Gerstein, M. (2006) The Database of Macromolecular Motions: new features added at the decade mark. *Nucleic Acids Res.* **34,** D296–301
24. Yengo, C. M., De la Cruz, E. M., Safer, D., Ostap, E. M., and Sweeney, H. L. (2002) Kinetic characterization of the weak binding states of myosin V. *Biochemistry* **41,** 8508–8517
25. Yengo, C. M., and Sweeney, H. L. (2004) Functional role of loop 2 in myosin V. *Biochemistry* **43,** 2605–2612
26. Malnasi-Csizmadia, A., Woolley, R. J., and Bagshaw, C. R. (2000) Resolution of conformational states of *Dictyostelium* myosin II motor domain using tryptophan (W501) mutants: implications for the open-closed transition identified by crystallography. *Biochemistry* **39,** 16135–16146
27. Malnasi-Csizmadia, A., Kovacs, M., Woolley, R. J., Botchway, S. W., and Bagshaw, C. R. (2001) The dynamics of the relay loop tryptophan residue in the *Dictyostelium* myosin motor domain and the origin of spectroscopic signals. *J. Biol. Chem.* **276,** 19483–19490
28. Malnasi-Csizmadia, A., Pearson, D. S., Kovacs, M., Woolley, R. J., Geeves, M. A., and Bagshaw, C. R. (2001) Kinetic resolution of a conformational transition and the ATP hydrolysis step using relax-

ation methods with a *Dictyostelium* myosin II mutant containing a single tryptophan residue. *Biochemistry* **40,** 12727–12737
29. Geeves, M. A., and Holmes, K. C. (1999) Structural mechanism of muscle contraction. *Annu. Rev. Biochem.* **68,** 687–728
30. Gyimesi, M., Kintses, B., Bodor, A., Perczel, A., Fischer, S., Bagshaw, C. R., and Malnasi-Csizmadia, A. (2008) The mechanism of the reverse recovery step, phosphate release, and actin activation of *Dictyostelium* myosin II. *J. Biol. Chem.* **283,** 8153–8163
31. White, H. D., Belknap, B., and Webb, M. R. (1997) Kinetics of nucleoside triphosphate cleavage and phosphate release steps by associated rabbit skeletal actomyosin, measured using a novel fluorescent probe for phosphate. *Biochemistry* **36,** 11828–11836
32. Hannemann, D. E., Cao, W., Olivares, A. O., Robblee, J. P., and De La Cruz, E. M. (2005) Magnesium, ADP, and actin binding linkage of myosin V: evidence for multiple myosin V-ADP and actomyosin V-ADP states. *Biochemistry* **44,** 8826–8840
33. Rosenfeld, S. S., Houdusse, A., and Sweeney, H. L. (2005) Magnesium regulates ADP dissociation from myosin V. *J. Biol. Chem.* **280,** 6072–6079
34. Sasaki, N., Shimada, T., and Sutoh, K. (1998) Mutational analysis of the switch II loop of *Dictyostelium* myosin II. *J. Biol. Chem.* **273,** 20334–20340
35. Coureux, P. D., Wells, A. L., Menetrey, J., Yengo, C. M., Morris, C. A., Sweeney, H. L., and Houdusse, A. (2003) A structural state of the myosin V motor without bound nucleotide. *Nature* **425,** 419–423
36. Reck-Peterson, S. L., Tyska, M. J., Novick, P. J., and Mooseker, M. S. (2001) The yeast class V myosins, Myo2p and Myo4p, are nonprocessive actin-based motors. *J. Cell Biol.* **153,** 1121–1126
37. Rock, R. S., Rice, S. E., Wells, A. L., Purcell, T. J., Spudich, J. A., and Sweeney, H. L. (2001) Myosin VI is a processive motor with a large step size. *Proc. Natl. Acad. Sci. U. S. A.* **98,** 13655–13659
38. Takagi, Y., Yang, Y., Fujiwara, I., Jacobs, D., Cheney, R. E., Sellers, J. R., and Kovacs, M. (2008) Human myosin Vc is a low duty ratio, nonprocessive molecular motor. *J. Biol. Chem.* **283,** 8527–8537
39. Toth, J., Kovacs, M., Wang, F., Nyitray, L., and Sellers, J. R. (2005) Myosin V from *Drosophila* reveals diversity of motor mechanisms within the myosin V family. *J. Biol. Chem.* **280,** 30594–30603
40. Yang, Y., Kovacs, M., Sakamoto, T., Zhang, F., Kiehart, D. P., and Sellers, J. R. (2006) Dimerized *Drosophila* myosin VIIa: a processive motor. *Proc. Natl. Acad. Sci. U. S. A.* **103,** 5746–5751
41. De La Cruz, E. M., Ostap, E. M., and Sweeney, H. L. (2001) Kinetic mechanism and regulation of myosin VI. *J. Biol. Chem.* **276,** 32373–32381
42. Durrwang, U., Fujita-Becker, S., Erent, M., Kull, F. J., Tsiavaliaris, G., Geeves, M. A., and Manstein, D. J. (2006) *Dictyostelium* myosin-IE is a fast molecular motor involved in phagocytosis. *J. Cell Sci.* **119,** 550–558
43. Fujita-Becker, S., Durrwang, U., Erent, M., Clark, R. J., Geeves, M. A., and Manstein, D. J. (2005) Changes in Mg^{2+} ion concentration and heavy chain phosphorylation regulate the motor activity of a class I myosin. *J. Biol. Chem.* **280,** 6064–6071
44. Tsiavaliaris, G., Fujita-Becker, S., Durrwang, U., Diensthuber, R. P., Geeves, M. A., and Manstein, D. J. (2008) Mechanism, regulation, and functional properties of *Dictyostelium* myosin-1B. *J. Biol. Chem.* **283,** 4520–4527
45. Urbanke, C., and Wray, J. (2001) A fluorescence temperature-jump study of conformational transitions in myosin subfragment 1. *Biochem. J.* **358,** 165–173
46. Murphy, C. T., Rock, R. S., and Spudich, J. A. (2001) A myosin II mutation uncouples ATPase activity from motility and shortens step size. *Nat. Cell Biol.* **3,** 311–315
47. Yang, Y., Gourinath, S., Kovacs, M., Nyitray, L., Reutzel, R., Himmel, D. M., O'Neall-Hennessey, E., Reshetnikova, L., Szent-Gyorgyi, A. G., Brown, J. H., and Cohen, C. (2007) Rigor-like structures from muscle myosins reveal key mechanical elements in the transduction pathways of this allosteric motor. *Structure* **15,** 553–564
48. De La Cruz, E. M., Wells, A. L., Sweeney, H. L., and Ostap, E. M. (2000) Actin and light chain isoform dependence of myosin V kinetics. *Biochemistry* **39,** 14196–14202
49. Forgacs, E., Sakamoto, T., Cartwright, S., Belknap, B., Kovacs, M., Toth, J., Webb, M. R., Sellers, J. R., and White, H. D. (2009) Switch 1 mutation S217A converts myosin V into a low duty ratio motor. *J. Biol. Chem.* **284,** 2138–2149
50. Libby, R. T., Lillo, C., Kitamoto, J., Williams, D. S., and Steel, K. P. (2004) Myosin Va is required for normal photoreceptor synaptic activity. *J. Cell Sci.* **117,** 4509–4515
51. Wagner, W., and Hammer, J. A., 3rd (2003) Myosin V and the endoplasmic reticulum: the connection grows. *J. Cell Biol.* **163**, 1193–1196
52. Thomas, C., Fricke, I., Scrima, A., Berken, A., and Wittinghofer, A. (2007) Structural evidence for a common intermediate in small G protein-GEF reactions. *Mol. Cell* **25,** 141–149

Received for publication May 10, 2010.
Accepted for publication June 24, 2010.